Int. J. Multiphase Flow, Vol. 3, pp. 383–397. Pergamon/Elsevier, 1977. Printed in Great Britain.

LIQUID FLOW PATTERNS ABOUT BARBOTAGE BUBBLES

S. A. BARAKAT and G. E. SIMS
Mechanical Engineering Department, University of Manitoba, Winnipeg, Canada

(*Received* 10 *January* 1976)

Abstract—This paper summarizes the results of a flow visualization study on the liquid motion around barbotage bubbles during growth and departure. Flow patterns, as well as for the first time, instantaneous velocities, are reported as a function of time and location about the bubbles. The experiments, employing the hydrogen-bubble technique and high-speed cine photography, were with: water as the liquid, air as the bubbled gas, orifice diameters of 0.116 and 0.252 cm, and different air flow rates; the two limiting cases of constant supply pressure and constant volumetric flow rate were covered. It was found that the liquid around a barbotage bubble assumes two velocity maxima, the first an outward maximum during bubble growth and the second in the opposite direction approximately at the time of bubble departure; further, liquid velocities were found to be higher close to the bubbling site. Certain differences in liquid velocities between the constant pressure and constant flow cases are explained in terms of available theoretical solutions to the bubble growth rate. Qualitative comparisons of the barbotage liquid flow patterns and those recently reported for boiling flow patterns are also presented.

1. INTRODUCTION

Barbotage, the bubbling of gas into a liquid, is important in many operations involving the transfer of heat or mass in chemical equipment. A considerable literature exists on bubble formation, especially on departure volume and frequency; this literature, at least to 1970, has been thoroughly reviewed by Kumar & Kuloor (1970). To date, so far as the present authors are aware, no study has been reported which gives liquid flow patterns and velocities around a barbotage bubble during growth and departure.

The present paper reports such a study. A previous study (Barakat & Sims 1972) showed the combination of the hydrogen-bubble technique and high-speed cine photograph to be suitable for barbotage flow visualization, and this combination was used here. The experiments were performed with water as the liquid and air as the gas bubbled at two different rates through either a 0.116 or 0.252 cm orifice. The tests covered the two limiting barbotage cases of constant supply pressure and constant volumetric flow rate.

The relationship between boiling and barbotage is of great interest, as evidenced for example from the early works of Zuber (1959), Kutateladze & Moskvicheva (1959), and Wallis (1960) to the recent contributions such as that of Kutateladze & Malenkov (1974). The present paper presents a qualitative comparison of the flow field about a barbotage bubble with that about a boiling bubble as reported recently by Kutateladze & Mamontova (1973).

2. APPARATUS

2.1 *Test section*

The essentials of the experimental apparatus are shown in figure 1 and described below; a more detailed account may be found in Barakat & Sims (1975). The test section consisted of a cast polyester plate having a drilled orifice, of either 0.116 or 0.252 cm diameter, at its centre. Nine 0.0076 cm diameter platinum wires, to act as cathodes for the generation of hydrogen bubbles, were cast in the plate along a diameter at different distances on both sides of the orifice. The wires, the location of which is given in table 1, were trimmed and polished flush with the surface. The plate was fastened to the top of a 3000 cm^3 stainless steel plenum chamber with side connections for air inlet and electrical connections. Also fastened to the chamber was a $25 \times 25 \times 20$ cm glass bubbling tank with a brass base. During experiments, the tank was partially filled with water and high-speed cine photographs were taken perpendicular to the plate diameter on which the wires were located.

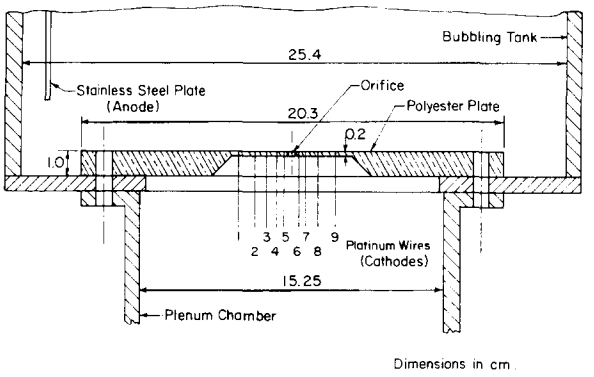

Figure 1. Test section.

Air was drawn from the building supply at 5.5 bars and was reduced in pressure to 0.7 bars (relative pressures) in passing through a pressure regulating valve. The air then passed through a filter, a moisture remover, a rotameter with a built-in needle valve, and finally through a saturator filled with distilled water.

The constant pressure conditions met the criteria proposed by Hughes *et al.* (1955); in this case, air was introduced into the plenum chamber. For the constant flow condition air was introduced through a glass capillary of the same inside diameter as the orifice and 25 cm long glued to the back of the plate and in line with the orifice; with the larger orifice (0.252 cm diameter), a porous disc (of 0.85 cm diameter and 0.2 cm thickness) was placed at the end of the capillary.

Table 1. Location of platinum wires

Wire No.	Distance from plate centre to centre-line of wire, cm 0.116 cm orifice	0.252 cm orifice
1	0.927	1.798
2	0.607	1.180
3	0.317	0.601
4	0.217	0.339
5	0.102	0.160
6	0.113	0.224
7	0.243	0.493
8	0.473	0.868
9	0.670	1.479

2.2 *Photographic equipment*

A 16 mm high-speed cine camera was used together with a timing-light generator for frame-rate determination. For illumination two 650 W (at 115 V) Smith Victor quartz–bromine movie lights were used at variable voltage; experiments showed that the clearest photographs of the hydrogen bubbles were obtained when photographed against a black background. Film stock was Kodak 4XR reversal in 100 ft rolls.

Developed films were projected on a viewer equipped with a digital XY reader of 0.13 mm resolution which allowed the accurate measurement of the X and Y location of any hydrogen bubble and of the air–bubble interface on each frame of the film.

3. EXPERIMENTAL CONDITIONS

The experimental conditions under which films were taken are given in table 2. The results are presented in detail in Barakat & Sims (1975) while in the present paper the results for one bubble typical of the constant pressure case (Bubble 54-2) and for one bubble typical of the

constant flow case (Bubble 64-15) will be presented with appropriate comments as to the effects of orifice size and flow rate.

All experiments were performed with air and water at room temperature (23°C). Distilled water was used with approx 0.4 g of sodium sulphate per litre of water added to increase the electrical conductivity of the water to about 7×10^{-4} mho/cm. The DC voltage applied to the wires ranged from 8 to 10 V depending on the water electrical conductivity. The air flow rate was adjusted to give single bubbles at either high or low frequency.

The air flow rates reported in table 2 were as measured by the rotameter except for low flow rates (below 0.4 cm^3/sec) which were out of the accurate range ofthe rotameter. For these small flows, the flow rates were determined from the films through the calculation of the air-bubble volume and frequency.

Table 2. Experimental conditions

Bubbling condition	Orifice size (cm)	Air flow (cm^3/sec)	Film No.
	0.116	0.47	56R3
Constant	0.116	5.58	57
pressure	0.252	1.2	54
	0.252	10.8	55
	0.116	0.021	58R2
Constant	0.116	0.102	63
flow rate	0.116	0.94	64
	0.252	0.07	62R
	0.252	0.58	61

4. RESULTS AND DISCUSSION

4.1 *Air-bubble behaviour*

Details regarding Bubbles 54-2 and 64-15, the bubbles analyzed in detail in this paper, are as follows:

	Bubble 54-2	Bubble 64-15
Condition	Constant pressure	Constant flow rate
Flow rate, cm^3/sec	1.2	0.94
Departure diameter, D_d, cm	1.501	0.385
Bubbling frequency of film, per sec	0.607	31.3
Departure time t_d, sec	0.053	0.026
Plenum chamber pressure, bars relative	0.013	—
Water height above surface, cm	12	7.3

As a test as to whether the air bubbles behaved as constant pressure or constant flow bubbles, bubble volumes and equivalent radii, (the equivalent radius is defined as the radius of a sphere of the same volume as the bubble) at various times during the bubble cycle were measured from the traced images using the method described by L'Ecuyer & Murthy (1965). Bubble growth rates and departure volumes were then compared with the previous experimental and theoretical results of Subash & Sims (1973) for constant pressure bubbling. This comparison is shown in figure 2 in the form of R/R_d plotted against t/t_d where: t is the time, t_d is the time at bubble departure, R is the bubble radius at time t and R_d is the bubble radius at departure time (the time origin was taken to correspond to the frame prior to the one where the bubble first appeared as a meniscus). These authors, using an orifice of 0.253 cm in a stainless steel plate, observed well the criteria established by Hughes *et al.* (1955) for constant pressure bubbling. The comparison shows close agreement with previous experimental results; comparison of the present results with the theory of these authors showed good agreement as well. For the constant flow

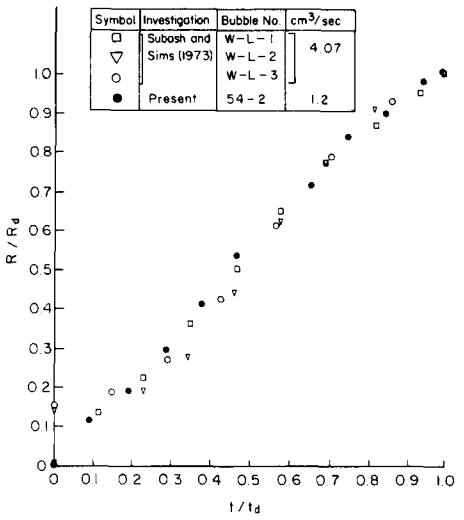

Figure 2. Bubble growth curves for the constant pressure condition.

conditions, bubble growth was also plotted in terms of R/R_d v. t/t_d in order to compare with the constant flow rate relation $R/R_d = (t/t_d)^{1/3}$; the comparison in figure 3 shows satisfactory agreement.

4.2 *Liquid flow pattern*

Air-bubble images along with the surrounding hydrogen-bubble trajectories representing the liquid flow pattern are given in figure 4 for Bubble 54-2 (constant pressure) and in figure 5 for Bubble 64-15 (constant flow rate). In these figures the Arabic numeral on each bubble image or hydrogen-bubble trajectory represents the number of the frame on the film, starting with frame 1 at initiation of the bubble, while the Roman numerals identify individual hydrogen-bubble trajectories. On each trajectory, unless specified to the contrary, the distance between two dots represents 3 frames in figure 4 and 10 frames in figure 5, which, knowing the framing rate, can be transformed into time intervals. The first dot on each trajectory is at bubble initiation and the small line perpendicular to the trajectory indicates the point of air-bubble departure. The line at the side of the air bubble represents the average rise of the hydrogen bubbles due to buoyancy during the time of the bubble cycle from initiation to departure (discussed in more detail in section 4.3).

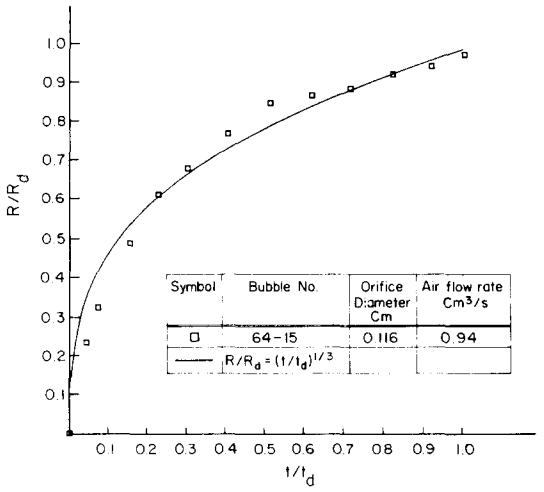

Figure 3. Bubble growth curves for the constant flow condition.

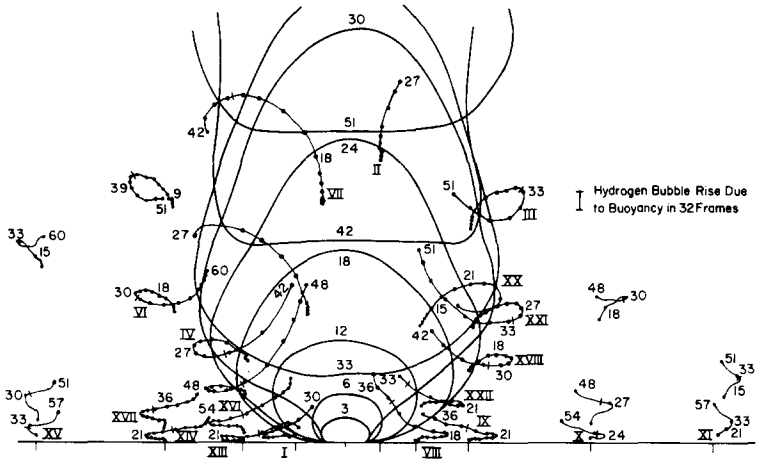

Figure 4. Hydrogen bubble trajectories about the constant pressure Bubble 54-2; departure at frame 32, film speed 600 pps.

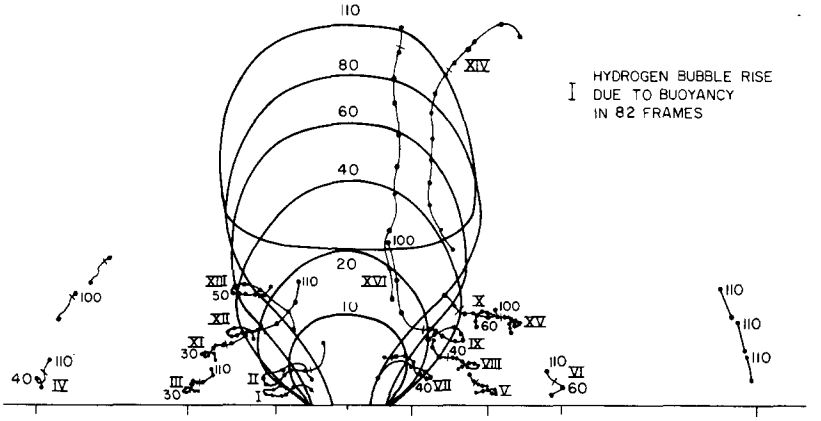

Figure 5. Hydrogen bubble trajectories about the constant flow Bubble 64-15; departure at frame 82, film speed 3350 pps.

4.2.1 *Flow about a constant pressure bubble.* As mentioned above, figure 4 gives the images of Bubble 54-2 generated at the 0.252 cm orifice for an air flow rate of 1.2 cm^3/sec and under constant pressure conditions. Generally, the analysis of constant pressure bubbles shows that during the initial bubble growth period liquid particles move radially away from the bubbling site due to the radial growth of the air–bubble interface. As the bubble cross-section diameter close to the plate surface reaches its maximum, the bubble starts to elongate vertically and this diameter begins to decrease from the maximum value; this causes the liquid particles to reverse their direction of motion and to move towards the centre, as for example, with Trajectories VIII and IX at approximately frames 19 and 21 respectively. The reversal in direction of motion propagates from the liquid particles close to the plate surface to those away from it as the bubble cross-section diameter at their level reaches a maximum; for example, Trajectory IX shows a direction reversal at frame 21, Trajectory XVIII at frame 25, Trajectory XXI at frame 28 and Trajectory III at frame 34 after bubble departure (the preceding frame numbers being approximate). As the air bubble forms a neck at the orifice and departs, liquid particles move upward in the wake of the bubble in a fashion that resembles a reversed stagnation flow, as evidenced, for example, by Trajectory VIII after frame 21, Trajectory XVIII after frame 30 and Trajectory XXI after frame 36.

The liquid motion propagates also in a radial direction on the plate surface but with a lag in time and a decrease in magnitude; this feature of the flow is discussed quantitatively later in the paper.

4.2.2 *Flow about a constant flow bubble.* Qualitatively, the same pattern of liquid motion was

observed about the air bubble generated under constant flow conditions, and as presented in figure 5. However, examination of liquid velocities, as performed below, will reveal differences in detail in comparison with the constant pressure case.

The flow pattern about both constant pressure and constant flow rate barbotage bubbles would appear qualitatively as in figure 6 where the dotted lines represent the motion during bubble growth, the solid lines near departure and the dashed lines after bubble departure. A qualitative correction has been made for buoyancy effects of the hydrogen bubbles.

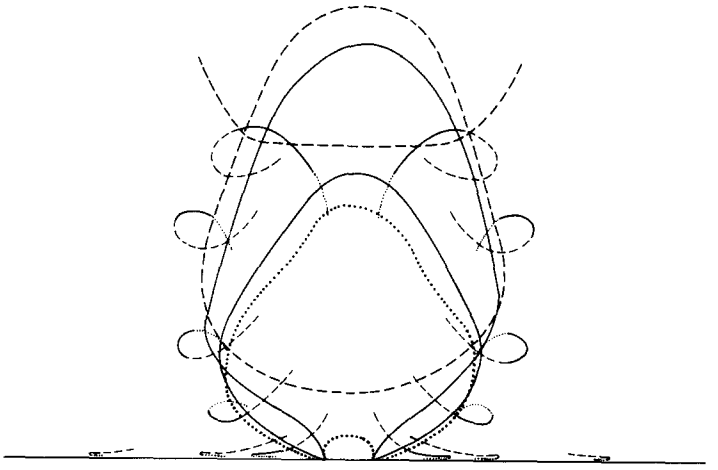

Figure 6. Schematic of liquid motion in the vicinity of a barbotage bubble.

4.3 *Liquid instantaneous velocities*

4.3.1 *Calculation of velocities.* Reading of the X and Y location of each hydrogen bubble at time intervals allowed the calculation of the instantaneous velocities of the liquid particles around the air bubble at the location of the hydrogen bubble as:

$$V_x = \frac{\Delta X}{n\Delta t},$$

$$V_y = \frac{\Delta Y}{n\Delta t} - V_{yb},$$

$$V_t = \sqrt{(V_x^2 + V_y^2)},$$

where: V_x = x-component of velocity, cm/sec;
V_y = y-component of velocity; it is meant to approximate the y-component velocity of the hydrogen bubble in the absence of buoyancy effects, cm/sec;
V_t = total velocity or magnitude of the velocity vector, cm/sec;
ΔX = distance traversed between two successive X readings, cm;
ΔY = distance traversed between two successive Y readings, cm;
n = number of frames between two successive readings;
Δt = time of single frame = 1/film speed, sec;
V_{yb} = vertical velocity of hydrogen bubbles due to buoyancy, cm/sec.

The hydrogen bubble rise velocity due to buoyancy V_{yb} was measured during the air bubble waiting period to eliminate the influence of the rising bubble. Also, especially for the higher frequency bubbling, V_{yb} was measured for the bubbles generated at the outermost wire where the liquid is less disturbed by the rising air bubbles. However, to check the values of V_{yb} and to be certain they did not include any component due to the air-bubble induced motion, an extra film

was photographed for the rising hydrogen bubbles with no air bubble generated at the orifice. It was found that, for the same hydrogen-bubble size, V_{yb} measured from the above-mentioned film was within 10% of values measured from other films.

Since V_{yb} depends on the hydrogen-bubble size, an average value was calculated for each film and used in the V_y calculation. The maximum difference between the extremes and the average value of V_{yb} was of the order of 30% for the same film. Typical hydrogen bubbles ranged from 0.008 to 0.025 cm in diameter depending on the water conductivity and the applied voltage. The average values of V_{yb} for Films 54 and 64 were 1.83 and 1.15 cm/sec respectively.

The velocity results are given in figures 7 to 12; first for constant pressure, the x-velocity close to the plate surface is presented, then the maximum x-velocities as a function of X/D_d, followed by total velocities at greater distances from the plate surface; the same quantities are then presented for the constant flow case.

4.3.2 *Liquid velocities around a constant pressure bubble.* Figure 7 presents the instantaneous velocity of liquid particles close to the plate surface at the R.H.S. of the bubble. The specification

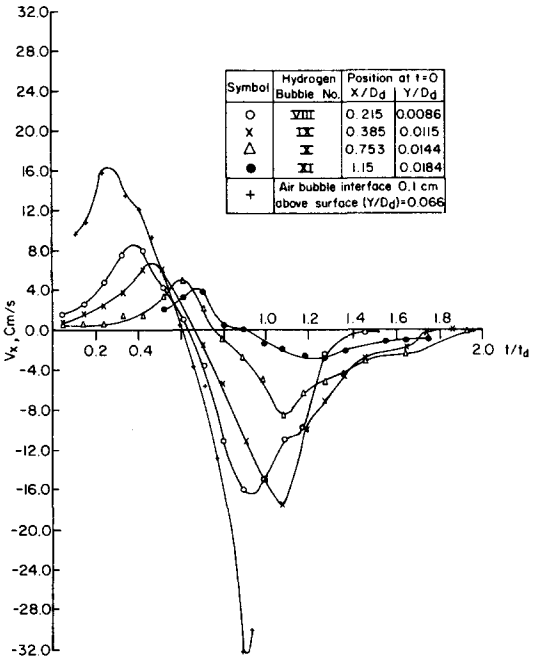

Figure 7. Liquid x-component velocity close to the plate surface about the constant pressure Bubble 54-2.

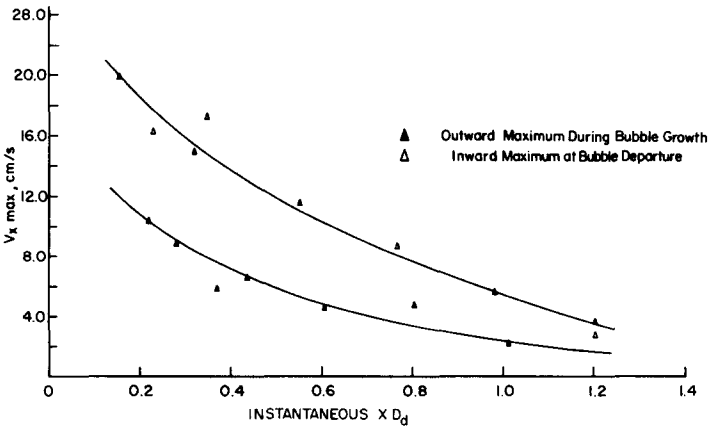

Figure 8. The change in the maximum x-component velocity close to the plate surface with distance from centre for the constant pressure Bubble 54-2

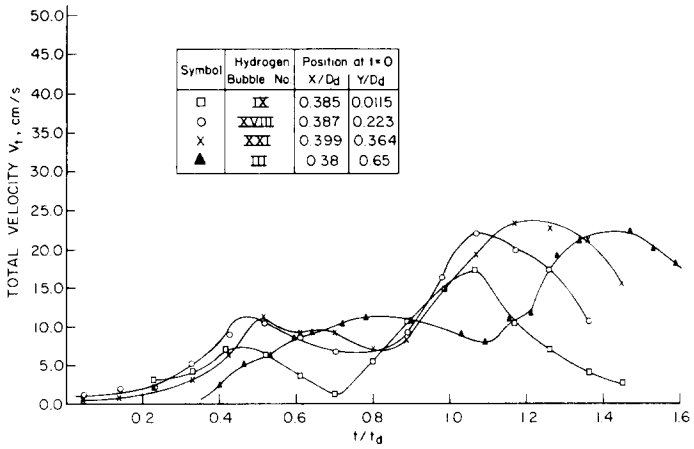

Figure 9. Total liquid velocity at levels away from the plate surface for the constant pressure Bubble 54-2.

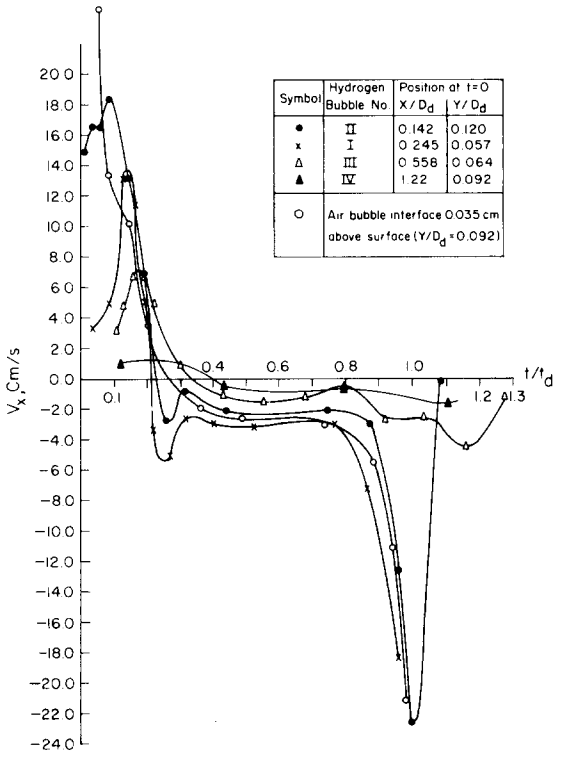

Figure 10. Liquid x-component velocity close to the plate surface for the constant flow Bubble 64-15.

"close to the plate surface" generally means locations 0.05 cm or less from the plate surface, that is $Y/D_d < 0.03$ for the constant pressure bubble and $Y/D_d < 0.13$ for the constant flow bubble. The figure shows that between initiation and t/t_d of 0.3–0.6 (depending on the liquid particle's radial location) liquid particles close to the plate surface accelerate outward as the air–bubble interface near the surface increases in diameter. The x-direction velocity V_x then reaches a maximum and begins to decrease as the bubble interface approaches its maximum diameter as represented by zero interface velocity at approx t/t_d of 0.6. At t/t_d between 0.65 and 0.85, liquid particles reach their zero V_x-value and they start accelerating towards the bubbling site as the air bubble reduces in cross-section diameter at the base forming a neck. A higher, but inward-direction x-velocity peak is reached approximately at or after bubble departure, here again depending on the distance from the centre. As the air bubble rises in the liquid, the liquid

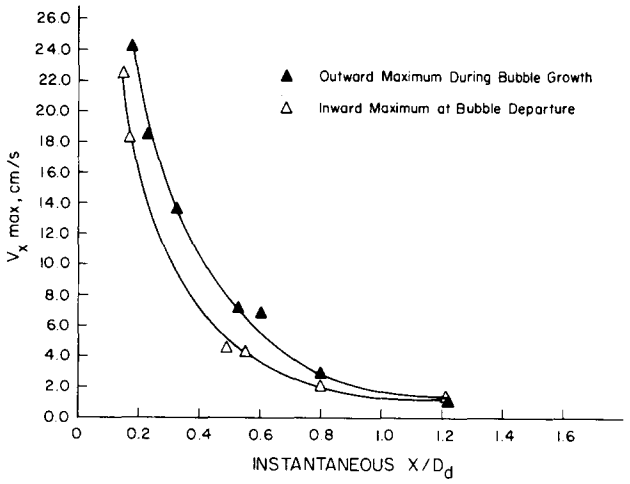

Figure 11. The change in the maximum x-component velocity close to the plate surface with distance from centre for the constant flow Bubble 64-15.

particles near the plate surface decelerate as they move in the wake of the bubble until they reach a zero V_x-value at t/t_d of 1.5–2.0.

It was observed that all liquid particles close to the surface go through the same motion pattern, but with decreasing velocity magnitudes with increasing distance from the bubbling site, and also with a time lag. This is illustrated especially by Trajectories VIII, X and XI in figure 7 whose positions may be located in figure 4.

The decay in $V_{x,max}$ and $V_{t,max}$ the maximum values of V_x and V_t respectively for the trajectory under consideration, close to the plate surface, with distance from the orifice for liquid particles on both sides of the air bubble is presented in table 3; X/D_d and Y/D_d values are those of the initial position of the hydrogen bubbles. In figure 8 $V_{x,max}$ is plotted against the instantaneous values of X/D_d at the time of each maximum; the figure also illustrates the consistently higher inward-direction maximum.

Total velocities of the liquid particles close to the surface were observed to show the same behaviour as V_x except that they do not reach a zero-value at points of direction reversal since a small vertical velocity component V_y exists. Table 3 illustrates the small differences existing between the values of $V_{x,max}$ and of $V_{t,max}$ at the various locations; the mean difference between the two values is of the order of 13.2%.

Table 3. Maximum velocities close to the plate surface around the constant pressure Bubble 54-2

Hydrogen bubble No.		Initial location X/D_d	Initial location Y/D_d	$V_{x,max}$ During growth	$V_{x,max}$ Near departure	$V_{t,max}$ During growth	$V_{t,max}$ Near departure
VIII	L.H.S. of bubble	0.215	0.0086	8.7	16.4	8.7	18.5
IX		0.385	0.0115	6.6	17.4	6.6	17.6
X		0.735	0.0144	5.0	8.4	5.0	8.5
XI		1.15	0.0184	3.8	2.8	3.8	3.0
I	R.H.S. of bubble	0.149	0.017	10.4	19.6	10.5	22.6
XIII		0.311	0.0086	6.4	14.4	6.4	14.4
XIV		0.558	0.0086	4.6	11.6	4.6	11.6
XV		0.95	0.02	3.4	5.8	3.4	6.0

Total velocities for liquid particles at approximately the same horizontal distance from the centre ($X/D_d \simeq 0.4$) but at different levels above the plate surface are presented in figure 9. The velocities at the different levels are generally of the same order of magnitude except that there

appears to be a tendency for the second maxima to be of larger magnitude at levels away from the plate surface than near the surface. There is also a lag in events (first maximum, minimum and second maximum) with distance from the surface. This phenomenon is illustrated by comparing the t/t_d of following events for Trajectories IX (initial $Y/D_d = 0.0115$) and III (initial $Y/D_d = 0.65$)

	t/t_d	
	Trajectory IX	Trajectory III
First maximum	0.44	0.81
Minimum	0.7	1.1
Second maximum	1.08	1.42

The sequence of these events and the dependence of timing on the distance from the plate surface is determined by the fact that, as mentioned earlier, liquid particles at a given level pass through a velocity maximum, then reverse their x-direction movement as the air-bubble horizontal diameter reaches a maximum at their particular level; they achieve their second maximum total velocity as they begin to move in the wake of the departing bubble. Also, due to the larger V_y values at levels away from the plate surface, the reduction in V_t due to V_x passing through zero at the time of direction reversal is largely reduced.

4.3.3 *Liquid velocities around a constant flow bubble.* The analysis of the flow around Bubble 64-15 is presented here as an example of the constant flow case. The variation of V_x close to the plate surface with time (t/t_d) is given in figure 10. The decay in V_x with distance from the centre is presented in table 4 and in figure 11 in the same manner as for the constant pressure bubble. Total velocities at different levels above the plate surface are given in figure 12.

Table 4. Maximum velocities close to the plate surface around the constant flow Bubble 64-15

	Hydrogen bubble No.	Initial position X/D_d	Initial position Y/D_d	$V_{x,max}$ During growth	$V_{x,max}$ Near departure	$V_{t,max}$ During growth	$V_{t,max}$ Near departure
L.H.S. of bubble	II	0.142	0.12	18.4	22.6	23.8	31.5
	I	0.245	0.057	13.8	18.4	14.6	21.2
	III	0.558	0.064	7.0	4.3	7.0	5.0
	IV	1.22	0.092	1.1	1.6	1.1	1.7
R.H.S. of bubble	VII	0.121	0.113	24.1	*	28.3	*
	V	0.485	0.069	7.4	4.5	7.5	4.7
	VI	0.797	0.065	2.7	2.3	3.0	2.3

*Hydrogen bubble joined with air bubble before a second velocity maximum was reached.

The velocity curves for the constant flow condition show approximately the same behaviour as for the constant pressure condition except for the following differences:

1. A constant flow bubble has a very high initial growth rate, as compared with constant pressure bubbles, with the first velocity maximum generated in the nearby liquid particles in the early stages of bubble formation around t/t_d of 0.1–0.2. The difference in bubble growth rate (dR/dt) for both conditions is demonstrated in figure 13 where the theoretical and the experimental growth rates are presented. The experimental values were obtained graphically by taking the gradient of the curve of bubble-equivalent-radius against time measurements. The method of generating the theoretical growth rate curves is to be found in the appendix.

2. For a substantial portion of the bubble growth ($0.3 < t/t_d < 0.85$) the liquid particle velocities are small, generally of the order of 4 cm/sec or less for the data shown; this is during the time when the bubble growth rate is low also, of the order of 8 cm/sec to 2 cm/sec with the bubble growth resulting mainly in an elongation in the vertical direction. The liquid particle

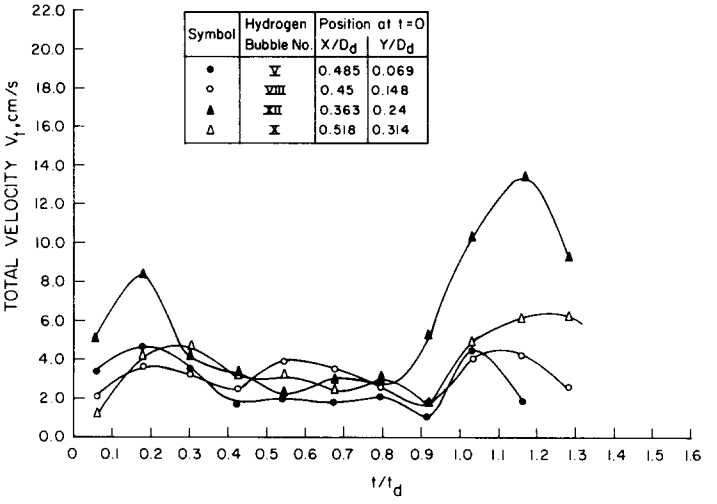

Figure 12. Total liquid velocity at levels away from the plate surface for the constant flow Bubble 64-15.

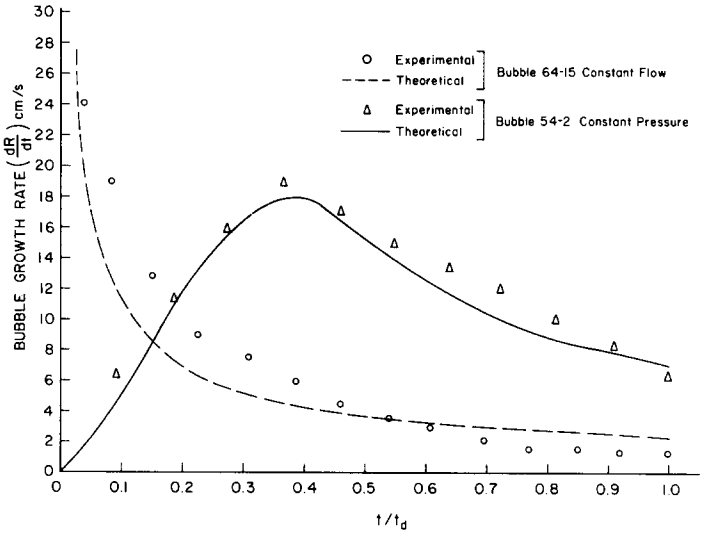

Figure 13. Bubble growth rates.

velocities remain at this magnitude until increasing to a maximum as the bubble forms a neck and departs.

3. While, for the constant pressure case, the second maximum is always higher than the first, this is not the case for all the constant flow bubbles. For example, figure 11 shows that the values of both velocity maxima for Bubble 64-15 are close in magnitude with the outward maximum at growth higher than the inward at departure with the larger difference being for liquid particles close to the bubble. This is, again, attributed to the high initial growth rate of the constant flow bubble. For bubbles generated at lower air flow rates the behaviour is the same as that for the constant pressure case.

4.4 *Effect of air flow rate and orifice diameter*

What follows will be somewhat qualitative, the detailed discussion will be found in Barakat & Sims (1975). In general, for both bubbling conditions, increasing the air flow rate was found to increase the velocity magnitudes, likely due, at least in the early stages of bubble growth, to the higher bubble growth rates themselves.

Although not conclusive, the present results (limited to two orifice diameters) suggest that

during bubble growth there are not large differences in velocities on changing the orifice diameter, while velocities near departure appear to be higher with the larger orifice.

As an indication of the limits of the values observed in the present experiments (see table 2), table 5 indicates the range of the maximum $V_{x,max}$ close to the plate surface and the maximum total velocity at levels away from the surface.

Table 5. Limits of velocities measured under experimental conditions

Phenomenon	Values in this paper for Bubble 54-2 or 64-15	Limits observed for whole of experimental program
Constant pressure bubbling		
Maximum measured values of $V_{x,max}$ close to the plate surface:		
During growth, cm/sec	10.4	6.6–13.0
Near departure, cm/sec	19.6	8.4–20.8
Maximum value of V_t away from plate surface at $X/D_d \simeq 0.4$ and $Y/D_d < 0.65$ cm/sec	24.0	24.0–29.5
Constant flow bubbling		
Maximum measured value of $V_{x,max}$ close to the plate surface:		
During growth, cm/sec	24.1	0.95–24.1
Near departure, cm/sec	22.6	7.8–22.6
Maximum value of V_t away from plate surface at $X/D_d \simeq 0.4$–0.5 and $Y/D_d < 0.61$, cm/sec	13.0	9.5–14.8

4.5 *Qualitative comparison with the liquid motion around a boiling bubble*

The flow pattern about the barbotage bubbles was examined in comparison with that about a boiling bubble as reported by Kutateladze & Mamontova (1973), who used tracer particles and high-speed cine photography in their study. The comparison is presented in figures 14 and 15 for the constant pressure bubble and the constant flow bubble respectively. In the comparison the bubble presented in figure 3 of the Kutateladze and Mamontova work (for saturated water boiling at 1 bar and 0.7×10^5 W/m^2) was used because the bubble profile at approximately departure is shown.

To construct each of the figures, the bubble images for boiling and barbotage (Bubbles 54-2 and 64-15) were magnified, with different magnification ratios, so that they all had the same apparent maximum horizontal diameter at departure. The boiling-bubble profile at departure (or

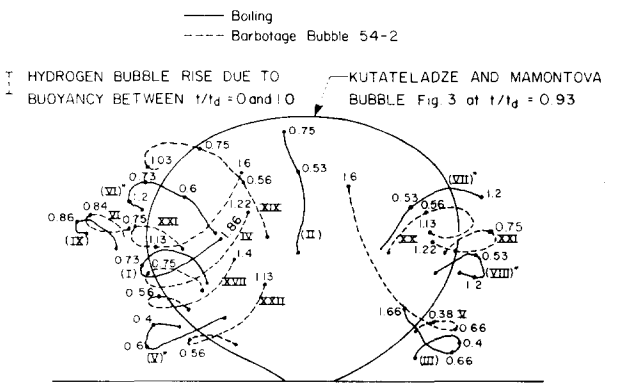

Figure 14. Comparison of flow pattern about a constant pressure barbotage bubble with that about a boiling bubble.

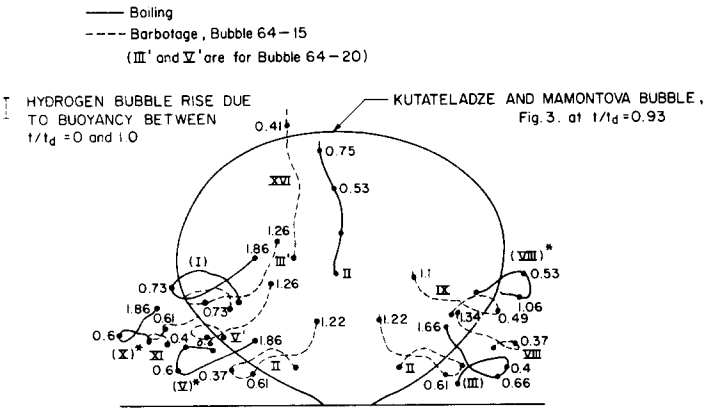

Figure 15. Comparison of flow pattern about a constant flow barbotage bubble with that about a boiling bubble.

more exactly at t/t_d of 0.93, one frame before departure) was then traced together with the particle trajectories around the bubble. The initial location (X and Y) of each particle was recorded as a ratio of X or Y to the bubble departure equivalent-diameter; the hydrogen bubbles with the closest initial X/D_d and Y/D_d ratios, from figure 4 for the constant pressure case and figure 5 for the constant flow case, were then located, and their trajectories reproduced on the boiling bubble. On each of figures 14 and 15 the Roman numerals in brackets refer to the particles around the boiling bubble; those marked with an asterisk were so labelled by the present authors while the rest carry the numbers used by Kutateladze & Mamontova (1973). The other Roman numerals (that is, those without brackets) identify the hydrogen bubble trajectories. For both boiling and barbotage, the trajectories begin at bubble initiation and various values of t/t_d are marked along the trajectories as an aid in comparing particle locations at different times. The average hydrogen-bubble rise due to buoyancy during a specified time period is also reported on the figure for each barbotage bubble.

Examination of figures 14 and 15 shows that, qualitatively speaking, the flow patterns about either a constant flow or a constant pressure bubble and boiling bubble are identical. For flow in the wake of the bubbles, the same qualititive similarities also exist. A more detailed quantitative comparison will be the subject of a further report.

5. CONCLUSIONS

1. For the first time, the motion of liquid in the vicinity of barbotage bubbles is reported in detail, both qualitatively and in terms of velocities for the two limiting cases of constant pressure and constant flow rate. Qualitatively, the liquid motion is summarized in figure 6.

2. Liquid velocities due to the bubble-induced motion are related to the bubble cycle. The liquid particles close to the plate surface have two velocity maxima, the first in the direction away from the bubbling site during the bubble growth and the second in the opposite direction about the time of bubble departure. Velocities near the plate surface decrease with increasing distance from the bubbling site.

3. Attention is drawn to the different character of the growth rate curves (dR/dt v $\cdot$ t/t_d) of constant pressure as opposed to constant flow bubbles as at least a partial explanation in interpreting the differences in liquid velocities around the two types of bubbles.

4. Qualitatively, the flow pattern about a barbotage bubble and that about a boiling bubble are essentially identical.

Acknowledgement—The authors gratefully acknowledge the support of the National Research Council of Canada by way of an operating grant to one of the authors (G.E.S.) and a scholarship to the other (S.A.B.).

REFERENCES

BARAKAT, S. A. & SIMS, G. E. 1972 High-speed cine-photography and oscillography in a boiling simulation, Proceedings of the 10th International Congress on High-Speed Photography, Nice, France, 486–490.

BARAKAT, S. A. & SIMS, G. E. 1975 Liquid flow patterns about barbotage bubbles, Dept. of Mech. Eng. Publication No. ER.25.24, The University of Manitoba, Winnipeg, Canada.

HUGHES, R. R., HANDLOS, A. E., EVANS, H. D. & MAYCOCK, R. L. 1955 The formation of bubbles at simple orifices. *Chem. Engng Prog.* **51**, 557–563.

KUMAR, R. & KULOOR, N. R. 1970 The formation of bubbles and drops, *in Advances in Chemical Engineering* (Edited by DREW T. B. *et al.*) Vol. 8, 255–368. Academic Press, New York.

KUTATELADZE, S. S. & MOSKVICHEVA, V. N. 1959 Hydrodynamics of a two-component layer as related to the theory of crises in the process of boiling. *Zh. Tekh. Fiz.* **29**, 1135–1139.

KUTATELADZE, S. S. & MAMONTOVA, N. N. 1973 The nature of motion of a liquid about a vapor bubble. *Heat Transfer, Soviet Res.* **5**, 149–153.

KUTATELADZE, S. S. & MALENKOV, I. G. 1974 Heat transfer at boiling and barbotage, similarity and dissimilarity, Proceedings of the Fifth International Heat Transfer Conference, Tokyo, **4**, Paper B1.1.

L'ECUYER, M. R. & MURTHY, S. N. B. 1965 Energy transfer from a liquid to gas bubbles formed at a submerged orifice, NASA TND-2547.

SUBASH, N. & SIMS, G. E., 1973, Bubble dynamics in barbotage and boiling, Mech. Eng. Dept., Publication No. ER.25.22, University of Manitoba, Winnipeg, Canada.

WALLIS, G. B. 1960 A gas–liquid analogue of nucleate boiling. *Nucl. Pwr* **5**, 99–101.

ZUBER, N. 1959 Hydrodynamic aspects of boiling heat transfer, Thesis. USAEC Report AECU-4439.

APPENDIX
THEORETICAL DETERMINATION OF THE BUBBLE GROWTH RATE

A.1 *Bubble growth rate under constant pressure conditions*

The method used in the present investigation was the same as formulated by Subash & Sims (1973). Combining the equation of motion for an expanding bubble (the Rayleigh equation) with the orifice equation results in the following dimensionless relation:

$$R^*\ddot{R}^* + 1.5\dot{R}^{*2} + 8ER^{*4}\dot{R}^{*2} + \frac{2}{R^*} = 2\Delta p^* \qquad [A.1]$$

where:

$$R^* \equiv R/R_0;$$

$$\dot{R}^* \equiv \frac{dR^*}{dt^*};$$

$$\ddot{R}^* \equiv \frac{d}{dt^*}\left(\frac{dR^*}{dt^*}\right);$$

$$t^* \equiv t\left[\frac{\sigma}{\rho_L R_0^3}\right]^{1/2};$$

$$\Delta p^* \equiv \left[\frac{p_1 - p_\infty}{2\sigma/R_0}\right];$$

$$E \equiv \frac{1}{K^2}\frac{\rho_g}{\rho_L};$$

R = radius of the bubble;
R_0 = radius of the orifice;
K = orifice constant;
P_1 = pressure in the plenum chamber;
P_∞ = pressure at a large distance from the bubble at the level of the orifice;
t = time;
σ = surface tension;
ρ_g = gas density;
ρ_L = liquid density.

The solution of the above equation was carried out by numerical integration, using the fourth order Runge–Kutta formula. The initial conditions were:

at time $t = 0$, $R^*(0) = 1$,
$\dot{R}^*(0) = 0$.

The solution results in finding the value of R^* and $\dot{R}^*$ as a function of t^* with Δp^* and E as parameters. Then, from the definitions of $\dot{R}^*$, t^*, Δp^* and E and a knowledge of the actual values of the physical quantities involved, the growth rate dR/dt v $\cdot$ t or t/t_d for the present Bubble 54-2 can be obtained; this is shown in figure 13.

Generally, especially in the early stages of growth, an increase in Δp^* results in higher values of the bubble growth rate. A higher Δp^* can be a result of higher gas flow rate generating a higher pressure drop.

A.2 *Bubble growth rate under constant flow conditions*

The equation representing a constant flow into the bubble is:

$$\frac{d}{dt}\left(\frac{4}{3}\pi R^3\right) = G \qquad [A.2]$$

where G is the value of the gas flow rate. That is,

$$\frac{dR}{dt} = \frac{G}{4\pi R^2}. \qquad [A.3]$$

The integration of [A.2] with $R = 0$ at $t = 0$ as initial condition would yield:

$$\frac{4}{3}\pi R^3 = Gt.$$

Substitution of R from this equation in [A.3] gives:

$$\frac{dR}{dt} = 0.2068\, G^{1/3} t^{-2/3}. \qquad [A.4]$$

The bubble growth rate can be calculated as a function of time from [A.4] for constant values of G; the curve for Bubble 64-15 is shown in figure 13. Equation [A.4] illustrates clearly the dependence of the growth rate on the air flow rate G.